WILEY

Research Article

Eco-Friendly Synthesis of CuO@ZnO Nanocomposites Using *Artemisia vulgaris* Leaf Extract and Study of Its Photocatalytic Activity for Methylene Blue

Pujan Nepal,[1] **Sandhya Parajuli,**[1] **Ganesh Prasad Awasthi,**[2] **Krishna Prasad Sharma,**[2] **Hari Bhakta Oli** ![ORCID],[1] **Ram Lal Shrestha** ![ORCID],[1] **and Deval Prasad Bhattarai** ![ORCID][1]

¹Department of Chemistry, Amrit Campus, Tribhuvan University, Kathmandu 44613, Nepal
²Division of Convergence Technology Engineering, Jeonbuk National University, Jeonju,
Jeollabuk-do, 54896, Republic of Korea

Correspondence should be addressed to Ram Lal Shrestha; swagatstha@gmail.com and Deval Prasad Bhattarai;
deval.bhattarai@ac.tu.edu.np

In this study, copper oxide nanoparticles (CuO NPs), zinc oxide nanoparticles (ZnO NPs), and copper oxide/zinc oxide nanocomposites (CuO@ZnO NPs) were synthesized by green synthetic route where bioactive compounds inherently present in the leaf extract of *Artemisia vulgaris* act as stabilizing and reducing agents. Phytochemicals present in leaf extract were assessed by qualitative chemical tests and spectroscopic measurements. UV-visible spectroscopy, Fourier Transform Infrared (FTIR) spectroscopy, Energy Dispersive X-ray (EDX) spectroscopy, X-ray Diffraction (XRD), and Field Emission Scanning Electron Microscopy (FESEM) were used to characterize the as-synthesized nanomaterials, i.e., CuO, ZnO, and CuO@ZnO NPs. XRD pattern revealed the crystalline nature of nanoparticles. Based on the Debye–Scherrer formula, the sizes of CuO NPs, ZnO NPs, and CuO@ZnO NCs were found to be 17.24, 20.74, and 22.50 nm, respectively. The band gap of the as-prepared nanomaterials was measured using the Tauc plot. Using the nanomaterials, MB degradation was studied at room temperature under exposure to UV light. The degradation efficiency of CuO, ZnO, and 2% CuO@ZnO was found to be 52%, 68%, and 98%, respectively. Kinetic degradation process reveals that the CuO@ZnO NCs showed a better photocatalytic activity on MB dye with the degradation constant of $0.04124 \, \text{min}^{-1}$ compared to those of either constituent. Based on the findings, it was found that CuO@ZnO nanocomposites have the potential to degrade MB as an organic dye and can be used for wastewater treatment.

1. Introduction

Organic dye is a major class of environmental contaminant in surface as well as groundwater systems [1]. These types of pollutants cause detrimental effects on human health as well as on the entire aquatic ecosystem due to their higher stability, persistent nature, and difficulty in the decomposition in the natural environment. Commonly used organic dyes include methylene blue (MB), methyl red, and Congo red [2]. Among these, methylene blue is commonly used as a dye to color paper, silk, wool, and cotton or stain indicator in various industries and biological science. After the uses, methylene blue remnants are released into the water streams which ultimately pollute the environment and ecological system [3]. MB has negative impacts on receiving water resources, and treating of MB dye is very crucial and of considerable interest. The increasing frequency of MB dyes in aqueous solution has emerged as one of the significant environmental contaminants. Presence of dyes in water develops color which is severely hazardous to aquatic life as it disrupts the photosynthesis and partially blocks the

sunlight irradiation. In humans, methylene blue is known to exhibit various harmful effects such as serotonin poisoning, bladder irritation, and lightheadedness [4].

Different methods of water purification, such as filtration, oxidation, adsorption, and photocatalytic techniques, have been developed [5–8]. One of the most effective methods for alleviating harmful organic pollutants is photocatalysis, a nicely shaped offshoot of sophisticated oxidation process [9]. Its effectiveness and economic viability are further attested by executing a low-cost resource, including semiconductor materials and photons for creating O_2^- and OH^- [10]. Recently, nanostructured semiconducting materials have been used as photocatalysts for the degradation of organic dyes or their oxidation into benign products [11, 12]. Pursuing the arguments, metal oxide nanoparticles such as TiO_2, ZnO, SnO_2, and Fe_2O_3 have been intensively studied as photocatalysts due to their appropriate band gap, high photocatalytic efficiency, and stability against optical corrosion. Basssim et al. synthesized ferric oxide nanoparticles through the green synthesis method using extract of *Citrus aurantium* and employed them for the degradation of MB [13]. Wang et al. exhibited that Graphdiyne composite TiO_2 nanofibers combat against implant infection through increased photocatasis and antibacterial ability [14]. Besides this, $ZnO/g-C_3N_4$ heterojunction photocatalysts and perovskite-type $NiTiO_3$ decorated with reduced GO and $g-C_3N_4$ nanosheets have been used for photocatalytic phenomenon [15, 16]. Amidst many nanoparticles, ZnO is superior in use because of its distinct advantages over others, such as direct band gap, simple customized structure, ease of crystallization, anisotropic growth, and higher exciton binding energy and electron mobility [10]. However, high recombination efficiency of photogenerated electrons and holes and the need for ultraviolet light with photon energy greater than the band gap energy limit its use. These key difficulties are required to be resolved in order for ZnO material to be used as a viable photocatalyst [17].

Many efforts have been made to improve the photocatalytic efficacy of ZnO nanostructures by changing their morphology, modifying ZnO with nonmetal doping, and adding transition metals or making composite [18]. The formation of nanocomposites is raising attention in the field of photocatalysis because of their stability, efficiency, and synergistic efforts [19]. In addition, formation of nanocomposite also widens the wavelength range for the materials to work in both UV and visible region. For this wider application, CuO@ZnO nanocomposite is at the forefront but its synthesis demands sophisticated instrumental and toxic chemicals [17, 20]. In this context, it is imperative to develop effective and efficient photocatalytic materials without causing detrimental effects on humans and the environment. In this direction, green synthesis of nanomaterials can be a good alternative in terms of cost, reliability, performance, and environmental friendliness.

In this method, nanomaterials are produced by utilizing nonhazardous, renewable, and low-cost raw materials. Preparation of large-scale materials with minimal contamination has resulted from the synthesis of nanomaterials employing a variety of sources, including bacteria, fungi, algae, and plants, due to growing popularity of green synthesis [21] which finds ways to create the best chemical products and processes under the aegis of the principle of green chemistry [22]. However, the synthesis of nanomaterials using bacteria, fungi, algae, and biological templates is limited because of their superspecificity towards nanoparticles. So, in the broad-spectrum synthesis of nanomaterials, plant extracts are highly recommended where phytochemicals in the extract act as reducing agents, capping agents, and stabilizing agents [23, 24].

Hitherto, the synthesis of CuO/ZnO nanocomposites (NCs) has been described utilizing plant extracts from various plant sources such as *Clerodendrum infortunatum* [25], *Melissa officinalis* L. [26], *Vaccinium arctostaphylos* L. [27], *Ginkgo biloba* [28], *V. sinaiticum* [5], *Aegle marmelos* [29], bark of *Theobroma cacao* [30], *Dovyalis caffra* [31], *Mentha longifolia* [7], and nettle leaf [32]. Though the processes were efficient and environmentally friendly, the percentage yield was found to be low. In addition, agglomerated nanomaterials were obtained from these methods. One of the reasons for this happening could be due to the selection of inappropriate reducing and stabilizing agents. Furthermore, the phytochemical constituents for the same chemical species may vary qualitatively and quantitatively with the variation of seasons, climate, and soil chemistry. In this work, a methanolic extract of *Artemisia vulgaris* leaf of Nepal origin has been used for the preparation of CuO@ZnO nanocomposite. Phytochemicals like flavonoids, triterpenoids, glycosides, polyphenols, saponins, and proteins are expected to serve as green product-based reducing agents as well as capping agents for the synthesis of CuO@ZnO nanocomposites. The degradation efficiency of CuO, ZnO, and 2% CuO@ZnO against methylene blue was found to be 52%, 68%, and 98%, respectively, exhibiting the best performance of as-prepared nanocomposite. As-prepared CuO@ZnO nanocomposites would be applicable for the photocatalytic degradation of other organic pollutants.

2. Experimental

2.1. Chemicals and Reagents. All the chemicals used in research, such as methanol (99.8%, EMPARTA), cupric nitrate trihydrate (99%, Qualigens), zinc nitrate hexahydrate (99%, Fisher Scientific), sodium hydroxide pellets (97%, LOBA CHEMIE), and methylene blue (70%, Fine-Chem), were of analytical grade and used in asreceived condition without further purification. The sample leaves of *Artemisia vulgaris* used in this study were collected from Sainamaina municipality ward No 11 ($27°41'31.9''$ N and $83°15'39.4''$ E), Rupandehi, Nepal, in September 2022.

2.2. Extract Preparation. *Artemisia vulgaris* leaves were washed with distilled water, dried in the shade for 10 days, and then crushed into a fine powder using a herbal medicine disintegrator (Model FW 177). The leaf extract was prepared by soaking 100 g of leaf powder in 750 mL methanol for 10 days followed by filtration.

2.3. Synthesis of Nanoparticles and Nanocomposites.

Firstly, 5.0 g of $Cu(NO_3)_2.3H_2O$ was taken and dissolved in 20 mL distilled water (DW). Then, the content was heated at 70°C under a constant magnetic stirring. While it was being stirred, 25 mL of plant extract was percolated into the solution, and 2 mL (5 M) NaOH was added to adjust the alkaline pH (pH~8.5) range, followed by stirring for 60 min. Subsequently, the mixture was sonicated for 10 minutes. After that, the mixture was centrifuged, filtered, and washed with distilled water (DW) and ethanol. Thus, the obtained precipitate was dried at 80°C for 12 h in vacuum and crushed to make powder with a mortar and pestle. Eventually, the powder form was calcined for 3 h at 400°C using a muffle furnace with a ramping rate of 5°C/min. The resulting product was labelled as CuO NPs.

For the synthesis of ZnO nanoparticles, 5.0 g of $Zn(NO_3)_2.6H_2O$ was taken, and a similar process for the synthesis of CuO NPs was applied. The resulting product was labelled as ZnO NPs.

Then, different percentage compositions of CuO@ZnO were synthesized in the same way.

For the synthesis of 50% CuO@ZnO nanocomposite, 2.5 g of $Cu(NO_3)_2.3H_2O$ and 2.5 g of $Zn(NO_3)_2.6H_2O$ were taken, and a similar protocol as mentioned in the synthesis of CuO NPs was applied. The resulting product was labelled as 50% CuO@ZnO NCs. CuO@ZnO nanocomposites of 2, 5, and 25% by weight of CuO were prepared using $Cu(NO_3)_2.3H_2O$ (0.1 g, 0.25 g, and 1.25 g) and $Zn(NO_3)_2.6H_2O$ (4.9 g, 4.75 g, and 3.75 g), respectively.

2.4. Physicochemical Characterization.

The phytochemical test of the methanolic extract of Artemisia vulgaris was based on the visual change upon chemical test. UV-visible spectroscopy was used to assess the formation of CuO NPs, ZnO NPs, and CuO@ZnO nanocomposites. The absorbance of the sample solution (at a concentration of 1 mg/10 mL distilled water) was measured using a double beam UV-visible spectrometer (Labtronics, model LT2802) in the wavelength range from 200 to 800 nm.

Fourier Transform Infrared (FTIR, PerkinElmer 10.6.2) Spectrometer was used to identify the functional group associated with the sample used as a stabilizing and reducing agent. The FTIR spectra were recorded at the cutoff range of $4000-400 \, cm^{-1}$ with a scan interval of $4 \, cm^{-1}$. The crystallinity and crystal phase of the obtained materials were probed by an X-ray diffraction (XRD, Rigaku diffractometer, Cu Kα, $\lambda = 1.5406 \, \text{Å}$) performed at JNCASR, Bengaluru, India. The crystal structure of the synthesized CuO, ZnO, and CuO@ZnO was examined in terms of peak intensities. The surface morphology of the composite materials was studied using Field emission scanning electron microscopy (FESEM, S-7400, Hitachi, Tokyo, Japan) equipped with energy dispersive X-ray spectroscopy (EDS). The transmission electron microscopy image of as-synthesized composite nanoparticles was studied using high-resolution transmission electron microscopy (HR-TEM, JEM-2200, JEOL, Ltd, Japan). Band gap of the materials was measured using a UV-Vis/NIR Spectrophotometer (Model: JASCO V-770, Japan).

2.5. Photocatalytic Activity.

Photocatalytic activities of the CuO/ZnO NCs were investigated by exposing 50 mL of 5 ppm methylene blue (MB) dye (Scheme 1) containing 30 mg of CuO/ZnO nanocomposite with constant magnetic stirring in a glass beaker under constant irradiation of UV light source (a series of six Philips UV lamps of 15 W power having a center wavelength of 254 nm positioned at 20 cm distant over the suspension surface). In order to ensure adsorption/desorption equilibrium, the solution was stirred for 30 min in the dark prior to the irradiation. The absorbance of the irradiated sample solution was recorded using a UV-visible double beam spectrophotometer in each 15-minute interval up to 90 minutes. The percentage of photocatalytic degradation (D %) was evaluated by using the following equation:

$$D \% = \frac{C_0 - C_t}{C_0} \times 100, \tag{1}$$

where C_0 and C_t represent the concentration of solution at initial ($t = 0$ min) and final (time = t).

3. Results and Discussion

3.1. Phytochemical Analysis.

A phytochemical test of the methanol extract of Artemisia vulgaris leaves was carried out in order to explore the possible reducing and capping agents for nanomaterial synthesis. The results obtained based on standard protocol (Supplementary information, Table S1) are shown in Table 1. These bioactive phytoconstituents were believed to act as reducing as well as stabilizing agents for the synthesis of nanomaterials. Similar findings are reported in a study by Thangjam et al. [33].

3.2. UV-Vis Spectroscopy Measurement.

UV-Vis spectroscopic measurement was performed to study the absorption pattern of as-synthesized nanoparticles. Figure 1(a) shows the UV-Vis spectra of CuO, ZnO, and CuO@ZnO nanocomposites. It is found that all of the produced materials, including ZnO, CuO, and CuO@ZnO, show absorbance at 325 nm. Nevertheless, the CuO@ZnO nanocomposites also exhibited shoulder peaks in UV-Vis spectra at around 430 nm. The red shift in the UV-Vis absorbance of the composite could be associated with relatively larger particle sizes of nanoparticles [32]. In comparison to ZnO, CuO and CuO@ZnO showed a broad peak. The absorption peaks widened with the percentage increase of CuO. It has been reported that the presence of CuO causes larger adsorption in the visible region [5].

3.3. Functional Group Analysis.

Functional groups present in plant extracts and remnants of such plant extracts in NPs or nanocomposites were studied by FTIR spectroscopy. The FTIR spectra of plant extract and synthesized nanostructure are shown in Figure 1(b). In the spectra of leaf extract, the broad spectrum at $3323 \, cm^{-1}$ was due to the O-H bond stretching. Similarly, the C–H stretching of alkane has resulted in a band at $2945 \, cm^{-1}$ and $2833 \, cm^{-1}$. Similarly, the C=O stretching of carbonyl compounds resulted in a band at
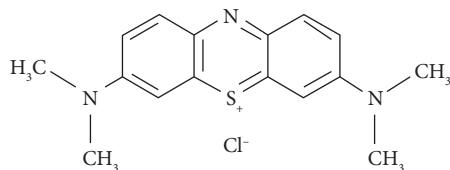
SCHEME 1: Structure of methylene blue.

TABLE 1: Phytochemicals present in the methanol extract of *Artemisia vulgaris* leaves.

Phytochemicals	Alkaloids	Flavonoids	Saponins	Terpenoids	Quinones	Polyphenols	Glycosides	Proteins
Results	−	+	+	+	+	+	+	+

+ sign indicates the presence, and − sign indicates the absence.
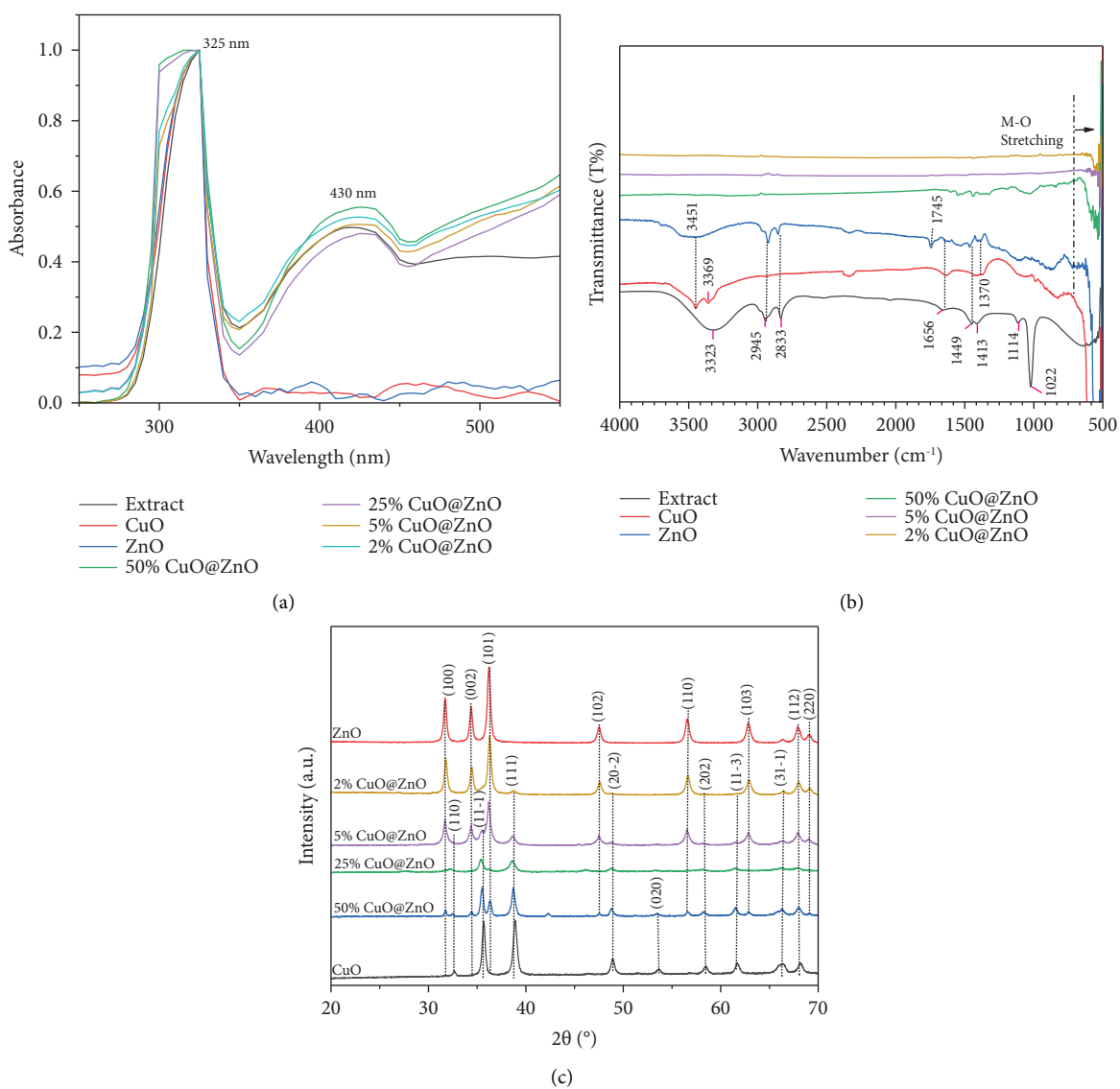

(a)

(b)

(c)

FIGURE 1: Physicochemical characterization: (a) UV-visible spectra of extract, CuO, ZnO, 50% CuO@ZnO, 25% CuO@ZnO, 5% CuO@ZnO, and 2% CuO@ZnO nanocomposites, (b) FTIR spectra of plant extract, as-synthesized CuO, ZnO, and CuO@ZnO NPS, and (c) XRD patterns of the as-synthesized samples—CuO, 50% CuO@ZnO, 25% CuO@ZnO, 5% CuO@ZnO, 2% CuO@ZnO, and ZnO.

$1656\,cm^{-1}$. The C–H bending of alkane gives rise to the band at $1449\,cm^{-1}$ and $1413\,cm^{-1}$. An absorption band at $1114\,cm^{-1}$ was ascribed to C-N stretching, and the band at $1022\,cm^{-1}$ was attributed to –C-O and –C-O-C- stretching of ester and tertiary alcohol. These assigned peaks were carried out in accordance with the spectrometric identification of organic compounds [34]. All in all, these peaks are indicative of their role as capping agents. The functionalities present in the methanolic extract of leaves of *Artemisia vulgaris* were found to be well indexed with some previously published reports [35].

In the spectra of ZnO NPs, O-H bond stretching of the phenolic group was observed at 3450 and $3369\,cm^{-1}$. The –OH group could be associated with the phytochemicals remnant with the nanoparticles. Likewise, the absorption band at $1745\,cm^{-1}$ and $1370\,cm^{-1}$ was attributed to C=C stretching of alkenes and stretching modes of nitrate anions, respectively.

In the same way, in the spectra of CuO NPs, the peak at $3451\,cm^{-1}$ was assigned as O-H stretching, $1656\,cm^{-1}$ as C=O stretching and $1465\,cm^{-1}$ as C-H bending [10, 36]. Furthermore, in all spectra of synthesized NPs and NCs, the bands that appeared in the range of $500–650\,cm^{-1}$ were assigned as metal-oxygen (M-O) stretching vibrations, which were well indexed to some reports [10].

3.4. Crystallinity Study. The crystallinity of the synthesized materials was examined by using XRD. The comparison of the XRD patterns of the as-synthesized nanostructure is shown in Figure 1(c). The XRD pattern of zinc oxide nanostructure appeared at 2θ values of 31.7°, 34.38°, 36.2°, 47.52°, 56.52°, 62.8°, and 67.9° which were well indexed to the (100), (002), (101), (102), (110), (103), and (112) planes of hexagonal ZnO, respectively, with JCPDS card no: 05–0664, space group: p6₃/mc, and cell constant: $a = b = 3.249\,\text{Å}$ and $c = 5.205\,\text{Å}$ [37]. Similarly, the XRD patterns of copper oxide nanostructure appeared at 2θ values of 32.62°, 35.70°, 38.88°, 48.92°, 53.34°, 58.40°, 61.7°, 66.46°, and 68.16° which were in good agreement to (110), (11-1), (111), (20-2), (020), (202), (11-3), (31-1), and (220) planes of monoclinic CuO, respectively, with JCPDS card no: 41–05682, space group: C_{12}/C_1, and cell constant: $a = 4.6949\,\text{Å}$, $b = 3.4382\,\text{Å}$, and $c = 5.187\,\text{Å}$ [38]. The diffraction peaks of CuO@ZnO at 2θ values matched with the diffraction peak of ZnO and CuO, confirming the formation of CuO@ZnO NCs.

The XRD patterns of these ZnO and CuO nanostructures showed no extra peaks, indicating that the materials were single-phase and, hence, extremely pure. Additionally, the Debye–Scherrer equation (2) was used to compute the average grain size of the zinc oxide, copper oxide, and composite nanoparticles [39].

$$D = \frac{K\lambda}{\beta\cos\theta},\qquad(2)$$

where D = crystallite size of materials; λ = wavelength of Cu Kα radiation (0.15406 nm); θ = Bragg's angle; β = corrected half width of the diffraction peak (in radian); and K = shape factor, which usually equals to 0.94.

The average grain size of as-synthesized CuO, ZnO, and CuO@ZnO nanostructures was found at around 17.24 nm, 20.74 nm, and 22.5 nm, respectively.

As seen in Figure 1(c), the intensity of ZnO peaks was significantly decreased with an increasing percentage of CuO in the CuO@ZnO nanocomposite structures. Hence, among the nanocomposites, the intensity of ZnO peaks was maximum at 2% CuO@ZnO nanocomposite, whereas the minimum was at 50% CuO@ZnO. Meanwhile, the intensity of CuO peaks increased with increasing percentage of CuO in the CuO@ZnO nanocomposite structures, and the intensity of the CuO peaks was found to be maximum at 50% CuO@ZnO while minimum at 2% CuO@ZnO nanocomposites. CuO peaks were found to be negligible for the amount less than that for 2% CuO@ZnO NCs. These findings are in good agreement with other findings [5, 7, 38, 40].

3.5. Surface Morphology Study. Surface morphology of as-prepared nanoparticles and nanocomposites was studied in terms of field emission scanning electron microscopy (FESEM) equipped with energy dispersive X-ray spectroscopy (EDS) and elemental mapping. As the MB adsorption or dye degradation occurs on the surface of nanomaterials, high surface area increases the photocatalytic activity. Therefore, nanostructured materials with high surface area can enhance the rate of photocatalytic activity. The surface morphology of as-synthesized CuO NPs, ZnO NPs, and 2% CuO@ZnO nanocomposite with various magnifications is shown in Figure 2. The images show the particles of nanosize dimension in agreement with those calculated using the Debye–Scherrer equation. Small size nanoparticles avail high surface area with affluent interparticle space which is useful for the channeling of MB solution in photocatalytic degradation process. As there is no significant aggregation of composite nanoparticles, the leaf extract of *Artemisia vulgaris* serves as a good capping agent.

Energy Dispersive X-ray spectroscopy (EDS) was employed to further demonstrate the presence of corresponding metal and oxygen in the composites as shown in Figures 3(a)–3(d). EDS layer mapping of different elements in as-synthesized 2% CuO@ZnO is shown in Figure 3(a). Figures 3(b)–3(d) represent the elemental mapping of the as-synthesized product, which revealed the presence of O, Zn, and Cu. The formation of nanocomposites is explicitly shown in the TEM image (Figures 3(e) and 3(f)). The particles seen in TEM image are explicitly within the nanorange domain. Figure 3(g) shows the EDS spectrum of the nanocomposites with the atomic percentage and weight percentage of each constituent element. Also, it shows a higher percentage of zinc (34.30 At %) compared to copper (4.79 At %) in the 2% CuO@ZnO nanocomposites. In a similar study, AbdulRazak et al. synthesized 3.5 wt% Cu-doped TiO_2 NPs and employed them for the degradation of anti-inflammatory drugs used by public health sector [41]. Compared to this finding, 2 wt% CuO@ZnO nanocomposites prepared in this research work reveal the formation of nanomaterials without any significant aggregation. In addition, the size of the nanomaterials in this work is smaller. This avails the higher surface area for the photocatalytic degradation of MB. Small size of
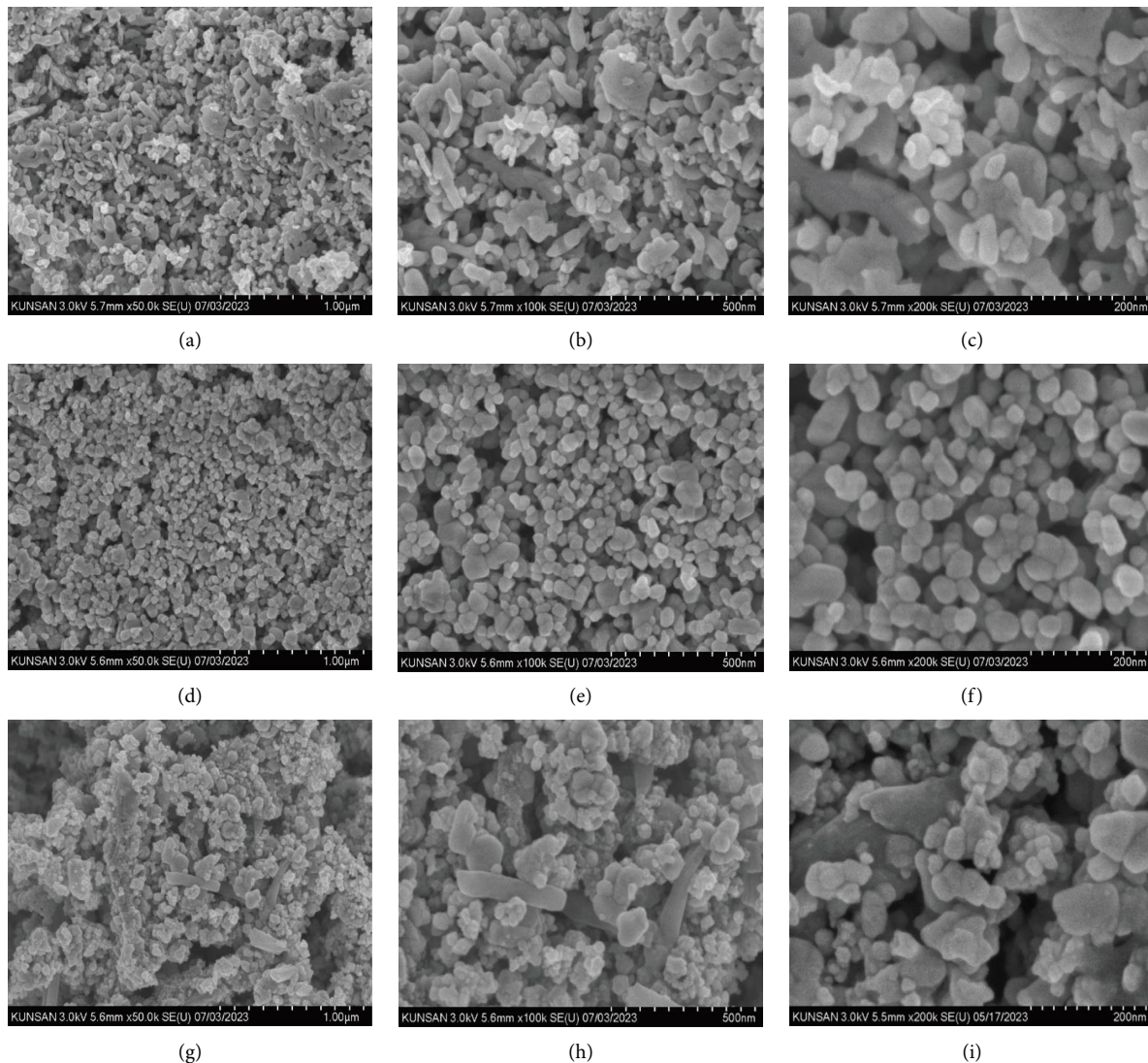
Figure 2: FESEM images with different magnifications of (a–c) CuO NPs, (d–f) ZnO NPs, and (g–i) 2% CuO@ZnO NCs, respectively. (a), (d), and (g) are of ×50 k magnification with a scale bar of 1 μm. (b), (e), and (h) are of ×100 k magnification with a scale bar of 500 nm. (c), (f), and (i) are of ×200 k magnification with 200 nm scale bar.

nanocomposites with high interparticle space can obviously avail the high surface area of the material which would be beneficial for surface catalytic phenomena such as photocatalytic degradation of MB dyes.

3.6. Band Gap Measurement.

In order to calculate the band gap energy of CuO NPs, ZnO NPs, and CuO@ZnO, a curve of $(\alpha h\upsilon)^2$ versus energy (eV) (Tauc plot) was plotted and fitted the linear region as shown in Figure 4. This shows that the band gap of 2% CuO@ZnO nanocomposites (2.93 eV) lies between that of CuO (1.62 eV) and ZnO (3.16 eV). This value of band gap energy corresponds to the visible light of lower frequency region.

3.7. Photocatalytic Activity

3.7.1. Wavelength Scanning.

The absorbance spectra of MB solution containing CuO, ZnO, and various ratios of CuO@ ZnO nanocomposites are shown in Figures 5(a)–5(f). A prominent peak at 665 nm of pure MB solution was recorded. Pure MB solution with the addition of different catalysts was subjected for 90 minutes to UV light irradiation. A subsequent decrease in the absorbance of the solution in each successive interval was observed. The rate of decrease in the absorbance of the solution with subsequent time intervals is different for different composites. For instance, the absorbance of MB solution at 0 minutes is about 1 absorbance unit. After 90 minutes, it is reduced up to half, i.e., up to 0.5 absorbance unit by ZnO. Similarly, for the same period, it is about 0.4 by CuO. Under the same condition, the absorbance is 0.24 for 50% CuO@ZnO and 0.16 for 25% CuO@ZnO nanocomposites. This is quite an improved condition but not significant. The rate of MB degradation for 5% and 2% CuO@ZnO is significantly more than others. Under the same exposure time, the absorbance shown by MB solution is 0.1 and 0.02 absorbance unit for 5% and 2%
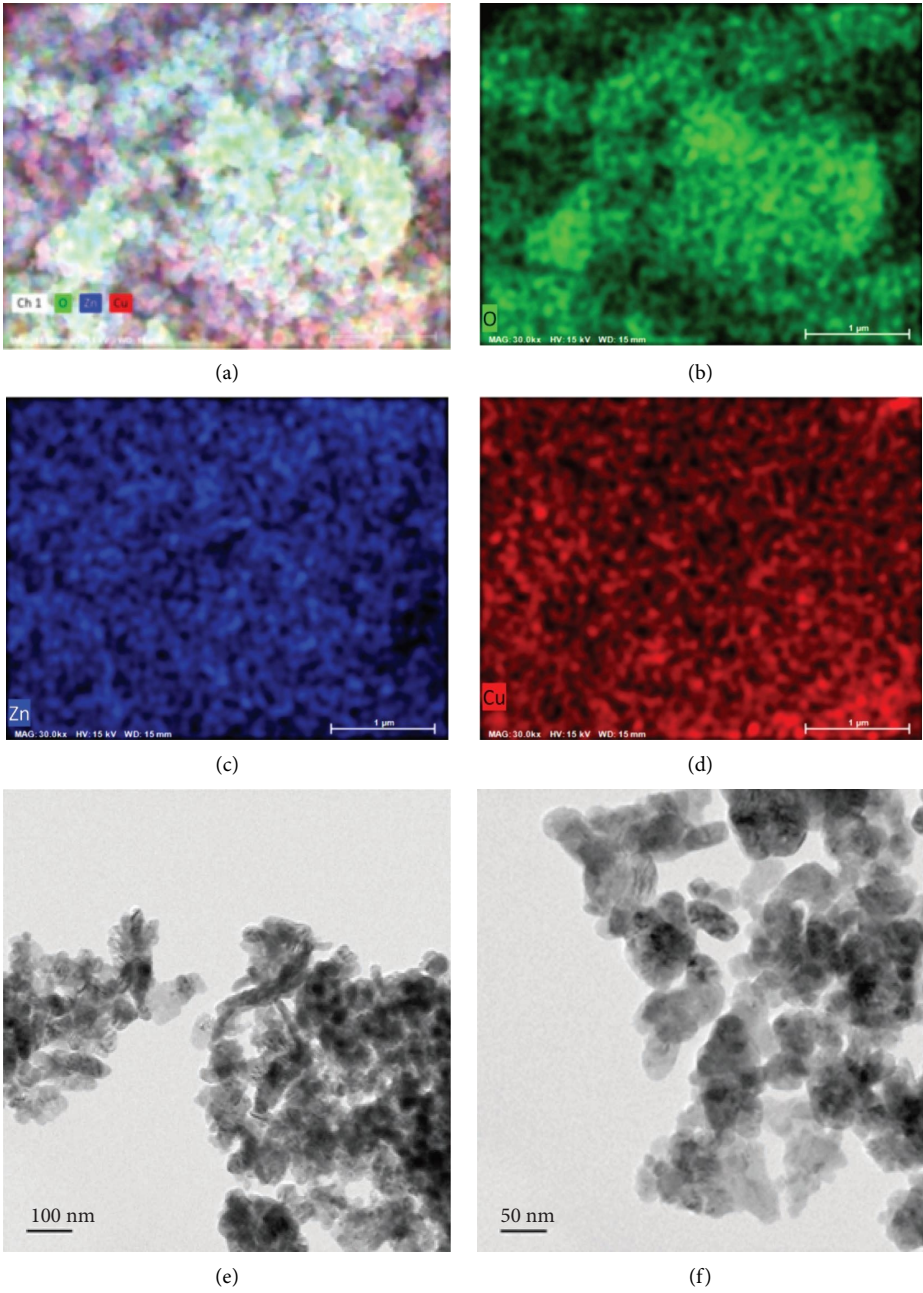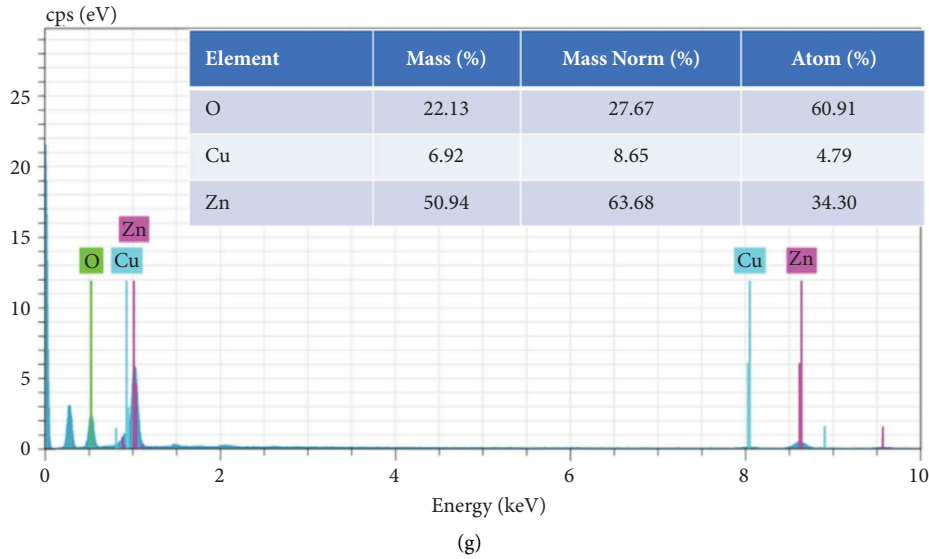
(a)

(b)

(c)

(d)

(e)

(f)

FIGURE 3: Continued.

(g)

FIGURE 3: Physicochemical characterization: elemental mapping of (a) Cu, Zn, and O,(b) O,(c) Zn, and (d) Cu in 2% CuO@ZnO NCs. (e-f) TEM image of 2% CuO@ZnO NCs under different magnification and (g) EDX spectrum of a typical 2% CuO@ZnO NCs.
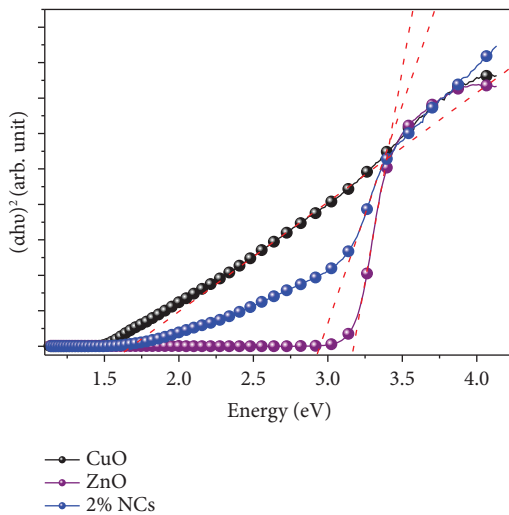

FIGURE 4: Tauc plot of different CuO, ZnO, and 2% nanocomposites of CuO@ZnO.

CuO@ZnO, respectively. From this observation, 2% CuO@ZnO is found to be the best-suited photocatalyst for the degradation of MB.

3.7.2. Photocatalytic Degradation and Degradation Efficiency.
Figure 6(a) illustrates the effect of copper concentration in the photodegradation of MB. The deterioration rate increased as the quantity of copper decreased, reaching its peak at 2% CuO@ZnO. Figure 6(b) compares the degradation efficiency at 90 min of all the green synthesized catalysts, evaluated using the following relation.

$$\text{Degradation efficiency } (D\%) = \frac{C_0 - C_t}{C_0} \times 100. \quad (3)$$

The order of degradation efficiency of different nanomaterials is as follows: CuO (52%) < ZnO (68%) < 50% CuO@ZnO (75%) < 25% CuO@ZnO (83%) < 5% CuO@ZnO (87%) < 2% CuO@ZnO (98%).

In comparison to bare ZnO NPs, all CuO@ZnO nanocomposites showed a better performance of photocatalytic degradation towards methylene blue. With a 98% degradation efficiency, 2% CuO@ZnO displayed the highest photocatalytic activity in this experiment. This shows a good result compared to other works regarding dye degradation (Table 2). It is believed that the coupling of CuO and ZnO to form a nanocomposite increases the photocatalytic performance by the mutual transfer of charge carriers, i.e., electron (e^-) and hole (h^+) from one semiconductor to another. This finding is also in good agreement with those of similar findings [44]. The transfer of e^- and h^+ from CuO to ZnO is energetically prohibited at higher amounts of CuO levels (50% CuO@ZnO), where the majority of photons may be directly absorbed by CuO. Thus, more amount of CuO in nanocomposites results in the reduction of superoxide anion radical production ($^\bullet O_2^-$) and the catalyst's degradation activity, whereas with a lower amount of CuO coating, NCs have significant potential to generate superoxide and hydroxyl radicals due to the potential of excited electron transfer from the conduction band of thin layer CuO to that of ZnO and transfer of holes from valence band of ZnO to that of CuO, which is also an energetically allowed process. Moreover, in moderate CuO-coated NCs, the production and reduction of superoxide radicals and hydroxyl radicals are both affected by the energetically preferred process of transfer of electrons and hole pairs [45–47]. Hence, it was found that the activity of the composite increased with a decreased amount of copper content.

3.7.3. Kinetic Degradation Process.
The kinetic equation can be expressed as $\ln (C_t/C_0) = -kt$, where k is the reaction rate constant, t is the time, C_t is the concentration of dye at
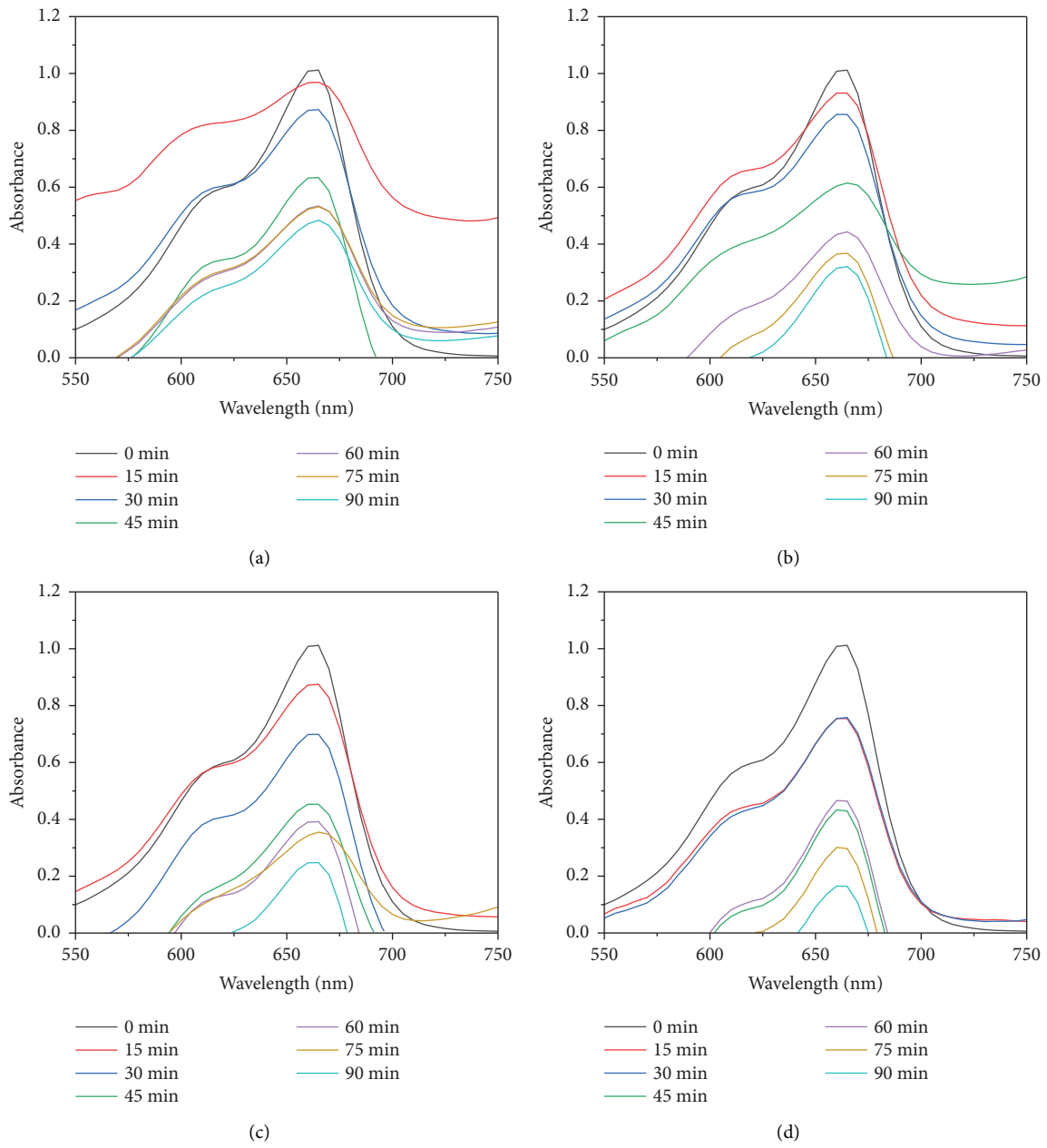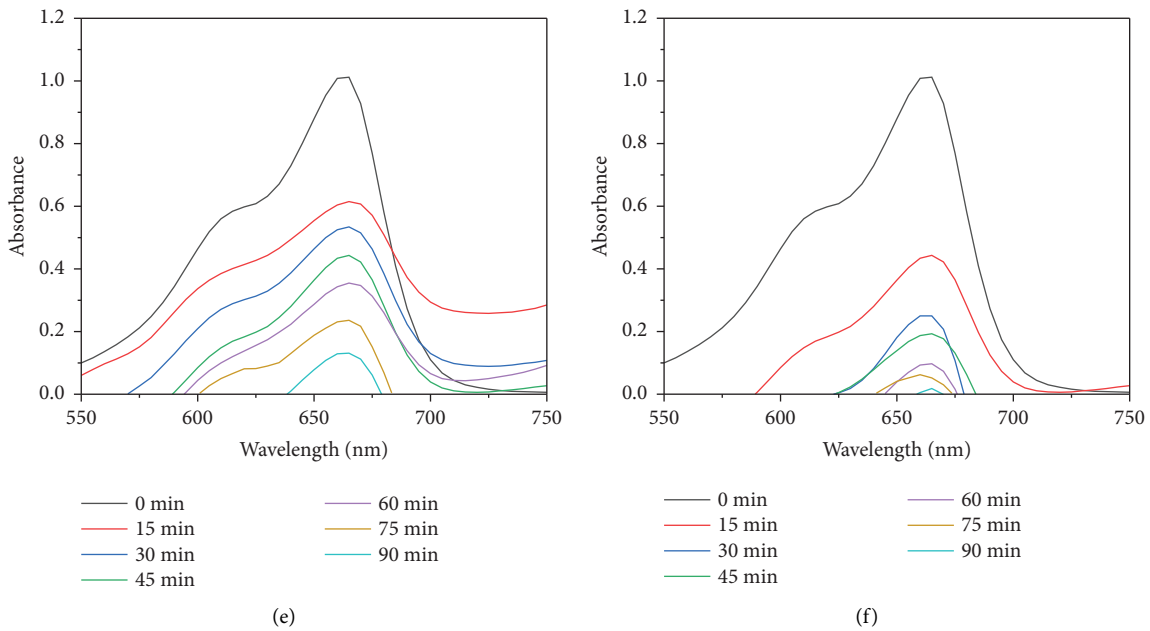
(a)

(b)

(c)

(d)

FIGURE 5: Continued.

(e)

(f)

FIGURE 5: Photocatalytic removal of MB using (a) CuO, (b) ZnO, (c) 50% CuO@ZnO, (d) 25% CuO@ZnO, (e) 5% CuO@ZnO, and (f) 2% CuO@ZnO.
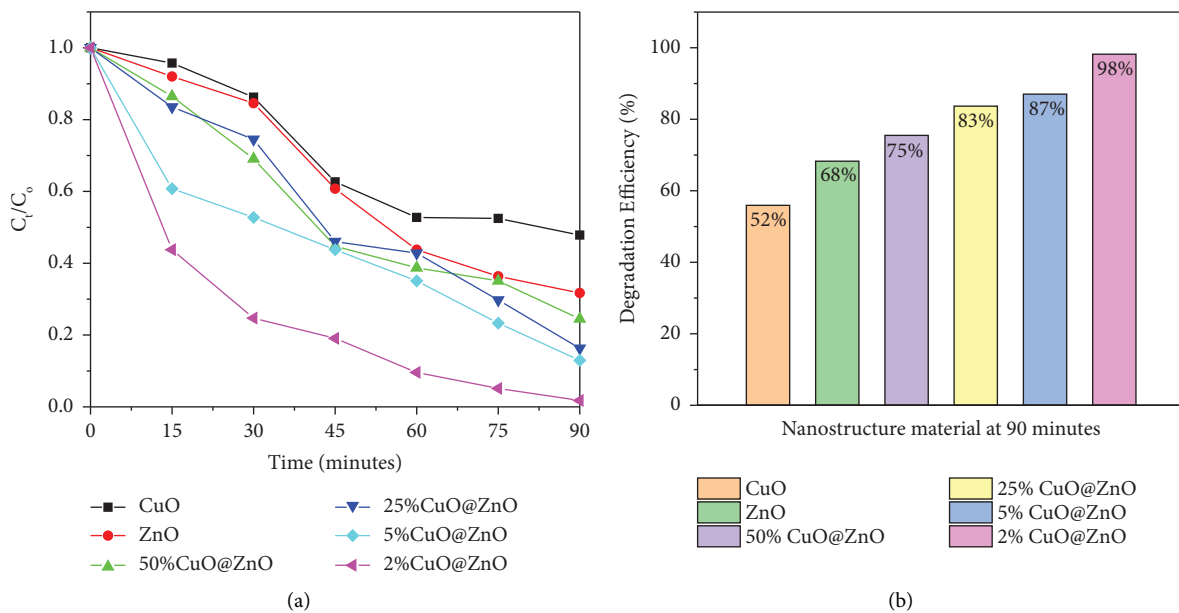

(a)

(b)

FIGURE 6: (a) Photocatalytic degradation of MB solution under UV light in the presence of different samples versus irradiation time. (b) Degradation efficiency of different nanostructured materials at 90 minutes.

different time intervals, and C_0 is the initial concentration of dye. The rate constant (k) calculated from the linear fitted plots of $\ln(C_t/C_0)$ versus time was found to be 0.0093, 0.01419, 0.01572, 0.01919, 0.02014, and 0.04124 min^{-1} for CuO, ZnO, 50% CuO@ZnO, 25% CuO@ZnO, 5% CuO@ZnO, and 2% CuO@ZnO NCs, respectively (Figure 7). The larger value of rate constant refers to the high photodegradation of MB dyes. The rate constant results suggest that the CuO@ZnO NCs showed a better photocatalytic activity on MB dye.

3.7.4. Degradation Mechanism. CuO@ZnO has a higher photocatalytic effectiveness than pure ZnO due to the interfacial charge separation and strong charge separation. Using a CuO@ZnO nanocomposite, the predicted process for improved dye photodegradation is put forth in Scheme 2. In this study, the green technique employing *Artemisia vulgaris* leaf extract may have created a heterojunction between the surfaces of ZnO and CuO semiconductors and triggered the photodegradation of dyes, which is a key component of the photocatalysis mechanism.

TABLE 2: A comparative study of pollutant degradation using photocatalysts.

| SN	Photocatalyst	Pollutants	Method of synthesis	Photodegradation efficiency (%)	Ref.
1	CuO/TiO$_2$ NPs	MB	Green synthesis using *Citrus aurantium* extract	98.6	[4]
2	Fe$_2$O$_3$ NPs	MB	Green synthesis using *Citrus aurantium* extract	93.14	[13]
3	Cu-doped TiO$_2$	Diclofenac sodium (DCF)	Chemical reduction method	96.5	[41]
4	Cu-doped TiO$_2$	Ibuprofen (IBN)	Chemical reduction method	94.2	[41]
5	Cu-doped TiO$_2$	Mefenamic acid (MFA)	Chemical reduction method	82.3	[41]
6	La-doped ZnO	MB	Coprecipitation	91.45	[42]
7	La-doped ZnO	Ciprofloxacin (CIP)	Coprecipitation	87.6	[42]
8	Fe$_3$O$_4$/chitosan NPs	MB	Green synthesis using *Moringa oleifera*	94.7	[43]
9	2% CuO@ZnO	MB	Green synthesis using leaf extract of *Artemisia vulgaris*	98	This work
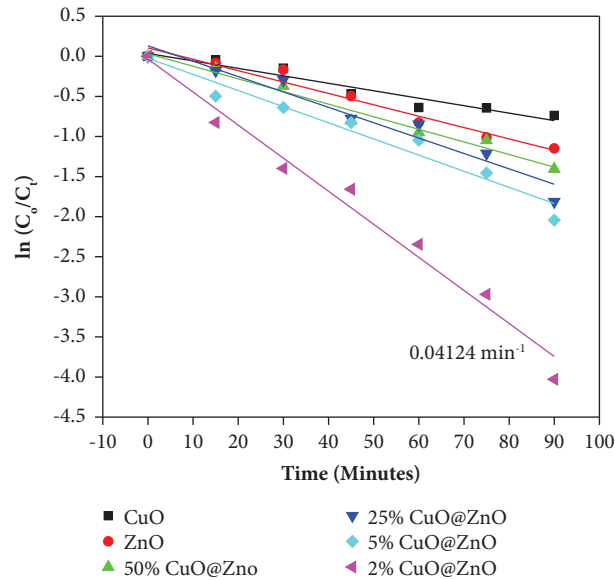
FIGURE 7: Kinetics of methylene blue degradation process.
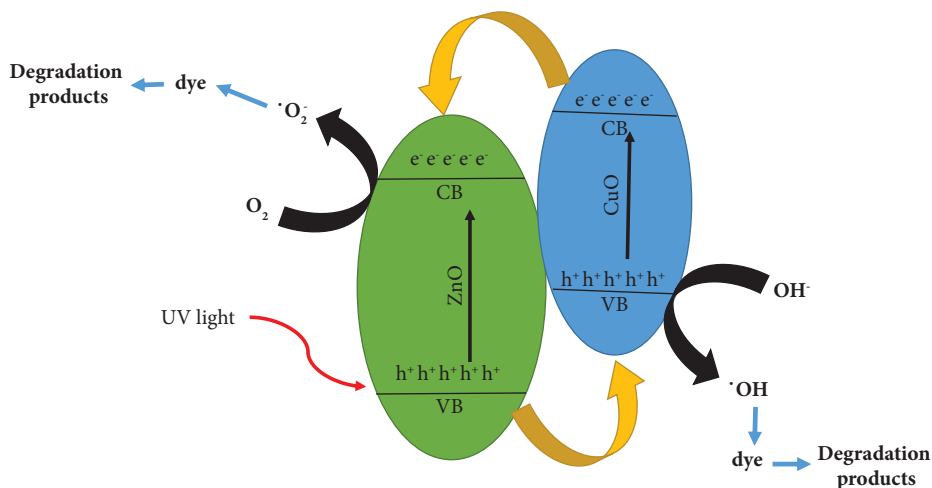
SCHEME 2: Possible degradation mechanism of CuO@ZnO photocatalyst under UV light.

The schematic diagram of the CuO@ZnO heterojunction's excitation and transfer of electrons and holes under UV light irradiation is shown in Scheme 2. The heterojunction created by CuO and ZnO helped to separate the photogenerated carriers [48].

ZnO and CuO were found to have valence band potentials of 2.42 and 1.43 ev, respectively, and conduction band potentials of -0.14 eV and -0.38 eV, respectively [28]. CuO is a narrow band gap semiconductor. In this work, the band gap of CuO and ZnO was found to be 1.62 eV and 3.16 eV, respectively. The band gap of 2% CuO@ZnO nanocomposites was found to be 2.93 eV which is sufficient to carry out the photoexcitation by the incident radiation of ~423 nm. The CuO@ZnO hollow sphere can produce photogenerated electrons and holes after irradiation by visible light. The location of conduction and valence bands of CuO is higher than those of ZnO, which is thermodynamically beneficial for the transfer of charge carriers created by light [49]. The photogenerated electrons will move from the conduction band of CuO to that of ZnO when exposed to UV radiation, whereas the photogenerated holes will move from the valence band of ZnO to that of CuO. Thus, due to the buildup of charge carriers like e^- in ZnO's conduction band and h^+ in CuO's valence band, the oxidation and reduction mechanisms over the surfaces of ZnO and CuO, respectively, result in the generation of superoxide ($\cdot O_2^-$) and hydroxyl ($\cdot OH$) radicals with the interaction of dissolved oxygen (O_2) and H_2O, respectively. The dye (MB) molecules engage in interactions with photogenerated radicals and fragment into more basic compounds. The dye molecules engage with photogenerated radicals and break down into smaller, less harmful organic compounds, which are then further transformed into CO_2 and water molecules, respectively [50].

4. Conclusions

Highly efficient CuO@ZnO NCs have been successfully synthesized via green synthetic route using the leaf extract of *Artemisia vulgaris* through a cost-effective, environmentally friendly, and nonhazardous method. Thus, synthesized CuO@ZnO NCs have been found to show significant photocatalytic degradation of methylene blue (MB). The degradation efficiency of CuO, ZnO, 50% CuO@ZnO, 25% CuO@ZnO, 5% CuO@ZnO, and 2% CuO@ZnO was found to be 52%, 68%, 75%, 83%, 87%, and 98%, respectively. Since the nanocomposite with lower concentration of CuO coated on ZnO exhibited effective separation and transport of photo-induced electron-hole pairs than that of pure ZnO, the composite with the lower amount of CuO coated on ZnO nanostructures enhanced the yield of photocatalytic degradation as compared to the higher amount of CuO coated on ZnO nanostructures. Inspired from the result, it is revealed that blending of high-cost copper materials with relatively low-cost zinc materials can offer several advantages in commercial production. Further optimization and some more detail tasks will be considered in the upcoming research. Therefore, based on the finding, it is found that 2% CuO@ZnO nanocomposites have the potential to degrade MB as an organic dye and can be used for wastewater treatment.

Data Availability

The data used to support the findings of this study are available from the authors/corresponding authors upon request.

Conflicts of Interest

The authors declare that they have no conflicts of interest.

Acknowledgments

Supplementary Materials

It includes the phytochemical analysis protocol. Results based on this protocol are included in this paper (Table S1). (*Supplementary Materials*)

References

[1] C. Valli Nachiyar, A. D. Rakshi, S. Sandhya, N. Britlin Deva Jebasta, and J. Nellore, "Developments in treatment technologies of dye-containing effluent: a review," *Case Studies in Chemical and Environmental Engineering*, vol. 7, 2023.

[2] H. Lachheb, E. Puzenat, A. Houas et al., "Photocatalytic degradation of various types of dyes (alizarin S, crocein orange G, methyl red, Congo red, methylene blue) in water by UV-irradiated titania," *Applied Catalysis B: Environmental*, vol. 39, no. 1, pp. 75–90, 2002.

[3] S. Liu, H. Ge, C. Wang, Y. Zou, and J. Liu, "Agricultural waste/graphene oxide 3D bio-adsorbent for highly efficient removal of methylene blue from water pollution," *Science of the Total Environment*, vol. 628-629, pp. 959–968, 2018.

[4] S. Bassim, A. K. Mageed, A. A. AbdulRazak, and F. Al-Sheikh, "Photodegradation of methylene blue with aid of green synthesis of CuO/TiO2 nanoparticles from extract of citrus aurantium juice," *Bulletin of Chemical Reaction Engineering and Catalysis*, vol. 18, no. 1, pp. 1–16, 2023.

[5] A. G. Bekru, L. T. Tufa, O. A. Zelekew, M. Goddati, J. Lee, and F. K. Sabir, "Green synthesis of a CuO–ZnO nanocomposite for efficient photodegradation of methylene blue and reduction of 4-nitrophenol," *ACS Omega*, vol. 7, no. 35, pp. 30908–30919, 2022.

[6] Z. Carmen and S. Daniel, "Textile organic dyes-characteristics, polluting effects and separation/elimination procedures from industrial effluents-a critical overview," *Organic Pollutants Ten Years After the Stockholm Convention-Environmental and Analytical Update*, vol. 3, 2012.

[7] A. Fouda, S. S. Salem, A. R. Wassel, M. F. Hamza, and T. I. Shaheen, "Optimization of green biosynthesized visible light active CuO/ZnO nano-photocatalysts for the degradation of organic methylene blue dye," *Heliyon*, vol. 6, no. 9, 2020.

[8] M. F. Hamza, F. Y. Ahmed, I. El-Aassy, A. Fouda, and E. Guibal, "Groundwater purification in a polymetallic mining area (SW Sinai, Egypt) using functionalized magnetic chitosan particles," *Water, Air, and Soil Pollution*, vol. 229, no. 11, pp. 360–414, 2018.

[9] H. B. Oli, A. A. Kim, M. Park, D. P. Bhattarai, and B. Pant, "Photocatalytic fuel cells for simultaneous wastewater treatment and power generation: mechanisms, challenges, and future prospects," *Energies*, vol. 15, no. 9, p. 3216, 2022.

[10] M. Mansournia and L. Ghaderi, "CuO@ ZnO core-shell nanocomposites: novel hydrothermal synthesis and enhancement in photocatalytic property," *Journal of Alloys and Compounds*, vol. 691, pp. 171–177, 2017.

[11] Y. Nosaka and A. Y. Nosaka, "Generation and detection of reactive oxygen species in photocatalysis," *Chemical Reviews*, vol. 117, no. 17, pp. 11302–11336, 2017.

[12] C. B. Ong, L. Y. Ng, and A. W. Mohammad, "A review of ZnO nanoparticles as solar photocatalysts: synthesis, mechanisms and applications," *Renewable and Sustainable Energy Reviews*, vol. 81, pp. 536–551, 2018.

[13] S. Bassim, A. K. Mageed, A. A. AbdulRazak, and H. S. Majdi, "Green synthesis of Fe3O4 nanoparticles and its applications in wastewater treatment," *Inorga*, vol. 10, no. 12, p. 260, 2022.

[14] R. Wang, M. Shi, F. Xu et al., "Graphdiyne-modified TiO2 nanofibers with osteoinductive and enhanced photocatalytic antibacterial activities to prevent implant infection," *Nature Communications*, vol. 11, no. 1, p. 4465, 2020.

[15] H. H. El-Maghrabi, S. A. Younis, H. R. Ali, and A. A. Nada, "Solar-driven photocatalytic transformation of toluene to benzoic acid over perovskite-type NiTiO3 decorated with reduced GO and g-C3N4 nanosheets," *Journal of Environmental Chemical Engineering*, vol. 11, no. 2, 2023.

[16] B. Liu, C. Bie, Y. Zhang, L. Wang, Y. Li, and J. Yu, "Hierarchically porous ZnO/g-C3N4 S-scheme heterojunction photocatalyst for efficient H2O2 production," *Langmuir*, vol. 37, no. 48, pp. 14114–14124, 2021.

[17] L. Xu, Y. Zhou, Z. Wu, G. Zheng, J. He, and Y. Zhou, "Improved photocatalytic activity of nanocrystalline ZnO by coupling with CuO," *Journal of Physics and Chemistry of Solids*, vol. 106, pp. 29–36, 2017.

[18] K. Qi, X. Xing, A. Zada et al., "Transition metal doped ZnO nanoparticles with enhanced photocatalytic and antibacterial performances: experimental and DFT studies," *Ceramics International*, vol. 46, no. 2, pp. 1494–1502, 2020.

[19] R. Reshmy, E. Philip, R. Sirohi et al., "Nanobiocatalysts: advancements and applications in enzyme technology," *Bioresource Technology*, vol. 337, 2021.

[20] S. Das and V. C. Srivastava, "An overview of the synthesis of CuO-ZnO nanocomposite for environmental and other applications," *Nanotechnology Reviews*, vol. 7, no. 3, pp. 267–282, 2018.

[21] S. Ahmad, S. Munir, N. Zeb et al., "Green nanotechnology: a review on green synthesis of silver nanoparticles-An eco-friendly approach," *International Journal of Nanomedicine*, vol. 14, pp. 5087–5107, 2019.

[22] P. T. Anastas and J. C. Warner, "Principles of green chemistry," *Green Chemistry: Theory and Practice*, vol. 29, pp. 14821–14842, 1998.

[23] J. Daphne, A. Francis, R. Mohanty, N. Ojha, and N. Das, "Green synthesis of antibacterial silver nanoparticles using yeast isolates and its characterization," *Research Journal of Pharmacy and Technology*, vol. 11, no. 1, pp. 83–92, 2018.

[24] S. Pandya, S. Jani, A. Chavan et al., "Nanocomposites and IT'S application-review," *International Journal of Pharmaceutical Sciences and Research*, vol. 4, no. 1, pp. 19–28, 2013.

[25] S. A. Khan, F. Noreen, S. Kanwal, A. Iqbal, and G. Hussain, "Green synthesis of ZnO and Cu-doped ZnO nanoparticles from leaf extracts of Abutilon indicum, Clerodendrum infortunatum, Clerodendrum inerme and investigation of their biological and photocatalytic activities," *Materials Science and Engineering: C*, vol. 82, pp. 46–59, 2018.

[26] M. Bordbar, N. Negahdar, and M. Nasrollahzadeh, "Melissa Officinalis L. leaf extract assisted green synthesis of CuO/ZnO nanocomposite for the reduction of 4-nitrophenol and Rhodamine B," *Separation and Purification Technology*, vol. 191, pp. 295–300, 2018.

[27] R. Mohammadi-Aloucheh, A. Habibi-Yangjeh, A. Bayrami, S. Latifi-Navid, and A. Asadi, "Enhanced anti-bacterial activities of ZnO nanoparticles and ZnO/CuO nanocomposites synthesized using Vaccinium arctostaphylos L. fruit extract," *Artificial Cells, Nanomedicine, and Biotechnology*, vol. 46, no. sup1, pp. 1200–1209, 2018.

[28] D. Thatikayala and B. Min, "Ginkgo leaves extract-assisted synthesis of ZnO/CuO nanocrystals for efficient UV-induced photodegradation of organic dyes and antibacterial activity," *Journal of Materials Science: Materials in Electronics*, vol. 32, no. 13, pp. 17154–17169, 2021.

[29] N. Basavegowda, P. Somu, A. M. Shabbirahmed, L. A. Gomez, and J. J. Thathapudi, "Bimetallic p-ZnO/n-CuO nanocomposite synthesized using Aegle marmelos leaf extract exhibits excellent visible-light-driven photocatalytic removal of 4-nitroaniline and methyl orange," *Photochemical and Photobiological Sciences*, vol. 21, no. 8, pp. 1357–1370, 2022.

[30] Y. Yulizar, R. Bakri, D. O. B. Apriandanu, and T. Hidayat, "ZnO/CuO nanocomposite prepared in one-pot green synthesis using seed bark extract of Theobroma cacao," *Nano-Structures and Nano-Objects*, vol. 16, pp. 300–305, 2018.

[31] J. O. Adeyemi, D. C. Onwudiwe, and A. O. Oyedeji, "Biogenic synthesis of CuO, ZnO, and CuO–ZnO nanoparticles using leaf extracts of Dovyalis caffra and their biological properties," *Molecules*, vol. 27, no. 10, p. 3206, 2022.

[32] A. Kalia, M. Kaur, A. Shami et al., "Nettle-leaf extract derived ZnO/CuO nanoparticle-biopolymer-based antioxidant and antimicrobial nanocomposite packaging films and their impact on extending the post-harvest shelf life of guava fruit," *Biomolecules*, vol. 11, no. 2, p. 224, 2021.

[33] N. M. Thangjam, J. Taijong, and A. Kumar, "Phytochemical and pharmacological activities of methanol extract of Artemisia vulgaris L. leaves," *Clinical Phytoscience*, vol. 6, no. 1, pp. 72–78, 2020.

[34] R. M. Silverstein and G. C. Bassler, "Spectrometric identification of organic compounds," *Journal of Chemical Education*, vol. 39, no. 11, p. 546, 1962.

[35] E. E. Elemike, D. C. Onwudiwe, and M. Singh, "Eco-friendly synthesis of copper oxide, zinc oxide and copper oxide–zinc oxide nanocomposites, and their anticancer applications," *Journal of Inorganic and Organometallic Polymers and Materials*, vol. 30, no. 2, pp. 400–409, 2020.

[36] N. Karki, S. Neupane, D. K. Gupta, and A. P. Yadav, "Electrochemical study on the effect of polar and non-polar extract of Artemisia vulgaris on the corrosion inhibition of mild-steel in an acidic medium," *RSC Advances*, vol. 13, no. 11, pp. 7603–7613, 2023.

[37] G. Li, K. Zhang, M. A. Mezaal, R. Zhang, and L. Lei, "Effect of electrolyte concentration and depth of discharge for zinc-air fuel cell," *International Journal of Electrochemical Science*, vol. 10, no. 8, pp. 6672–6683, 2015.

[38] C. F. Smura, D. R. Parker, M. Zbiri, M. R. Johnson, Z. A. Gál, and S. J. Clarke, "High-spin cobalt (II) ions in square planar coordination: structures and magnetism of the oxysulfides $Sr_2CoO_2Cu_2S_2$ and $Ba_2CoO_2Cu_2S_2$ and their solid solution," *Journal of the American Chemical Society*, vol. 133, no. 8, pp. 2691–2705, 2011.

[39] A. H. Moharram, S. A. Mansour, M. A. Hussein, and M. Rashad, "Direct precipitation and characterization of ZnO nanoparticles," *Journal of Nanomaterials*, vol. 2014, pp. 1–5, 2014.

[40] A. A. M. Sakib, S. M. Masum, J. Hoinkis, R. Islam, and M. A. I. Molla, "Synthesis of CuO/ZnO nanocomposites and their application in photodegradation of toxic textile dye," *Journal of Composites Science*, vol. 3, no. 3, p. 91, 2019.

[41] M. Al-Jemeli, M. A. Mahmoud, H. S. Majdi, M. F. Abid, H. M. Abdullah, and A. A. AbdulRazak, "Degradation of anti-inflammatory drugs in synthetic wastewater by solar photo-catalysis," *Catalysts*, vol. 11, no. 11, p. 1330, 2021.

[42] A. S. Soares, F. P. Araujo, J. A. Osajima, Y. Guerra, B. C. Viana, and R. Peña-Garcia, "Nanotubes/nanorods-like structures of La-doped ZnO for degradation of methylene blue and ciprofloxacin," *Journal of Photochemistry and Photobiology A: Chemistry*, vol. 447, 2024.

[43] N. I. Istiqomah, N. I. Istiqomah, S. I. Budianti et al., "Magnetically separable and reusable Fe_3O_4/chitosan nanocomposites green synthesized utilizing Moringa oleifera extract for rapid photocatalytic degradation of methylene blue," *Results in Chemistry*, vol. 7, 2024.

[44] M. Gerawork, "Photodegradation of methyl orange dye by using Zinc Oxide – copper Oxide nanocomposite," *Optik*, vol. 216, 2020.

[45] T. Chang, Z. Li, G. Yun, Y. Jia, and H. Yang, "Enhanced photocatalytic activity of ZnO/CuO nanocomposites synthesized by hydrothermal method," *Nano-Micro Letters*, vol. 5, no. 3, pp. 163–168, 2013.

[46] S. Khanchandani, S. Kundu, A. Patra, and A. K. Ganguli, "Shell thickness dependent photocatalytic properties of ZnO/CdS core–shell nanorods," *Journal of Physical Chemistry C*, vol. 116, no. 44, pp. 23653–23662, 2012.

[47] M. T. Qamar, M. Aslam, I. M. Ismail, N. Salah, and A. Hameed, "Synthesis, characterization, and sunlight

mediated photocatalytic activity of CuO coated ZnO for the removal of nitrophenols," *ACS Applied Materials and Interfaces*, vol. 7, no. 16, pp. 8757–8769, 2015.

[48] S. Chabri, A. Dhara, B. Show, D. Adak, A. Sinha, and N. Mukherjee, "Mesoporous CuO–ZnO p–n heterojunction based nanocomposites with high specific surface area for enhanced photocatalysis and electrochemical sensing," *Catalysis Science and Technology*, vol. 6, no. 9, pp. 3238–3252, 2016.

[49] E. D. Sherly, J. J. Vijaya, and L. J. Kennedy, "Visible-light-induced photocatalytic performances of ZnO–CuO nano-composites for degradation of 2, 4-dichlorophenol," *Chinese Journal of Catalysis*, vol. 36, no. 8, pp. 1263–1272, 2015.

[50] P. Karnati, A. Haque, M. F. N. Taufique, and K. Ghosh, "A systematic study on the structural and optical properties of vertically aligned zinc oxide nanorods grown by high pressure assisted pulsed laser deposition technique," *Nanomaterials*, vol. 8, no. 2, p. 62, 2018.